Proceedings of the ASME 2017 International Design Engineering Technical Conferences & Computers and Information in Engineering Conference
IDETC/CIE 2017
August 6-9, 2017, Cleveland, OH, USA

DETC2017-68540

DESIGN OF A SPHERICAL ROBOT WITH CABLE-ACTUATED DRIVING MECHANISM

Ernur Karadoğan, Ph.D.
School of Engineering & Technology
Central Michigan University
Mount Pleasant, Michigan, USA
ernur.karadogan@cmich.edu

Brian P. DeJong, Ph.D.
School of Engineering & Technology
Central Michigan University
Mount Pleasant, Michigan, USA
b.dejong@cmich.edu

ABSTRACT

This paper presents the kinematics and dynamics of a spherical robot with a mechanical driving system that consists of four cable-actuated moving masses. Four cable-pulley systems control four tetrahedrally-located movable masses and the robot functions by shifting its center of mass to create rolling torque. The cable actuation decreases overall mass and, therefore, allow for less energy expenditure, as compared to other moving mass mechanisms that translate the masses by powered-screws. Additionally, the design allows the center of mass for the static (spherical shell, electronics, motors etc.) and dynamic mass (moving masses) to be at the geometric center at any given time, therefore has potential for tumbleweeding when needed. The derived equations of motion are verified by means of simulations.

KEYWORDS

Spherical robot, Cable-actuation, Kinematics, Dynamics.

1. INTRODUCTION

Spherical robots, which are mobile robots that travel by rolling on a spherical shell, have drawn attention due to their advantages over legged- and wheeled-robots. For instance, they have an inherent stability as they can be designed to move from any initial orientation. They can be designed as self-contained mechanisms in the sense that the propulsion system can be confined within the robot making them ideal for dangerous environments such as search & rescue operations that may require traversing in debris and military applications. Other applications include surveillance [1], space exploration missions [2], environmental screening [3], marine exploration [4], and child development [5]. Additionally, as any mobile robot, they can be programmed to receive commands from a remote location or move autonomously in environments based on sensor information.

There are several driving mechanisms that propel spherical robots based on sprung central member [6], car-driven spherical shell [7], moving masses [8-9], and conservation of angular momentum [10]. Among these driving principles, moving masses may be considered to be the most versatile due to its simple design, obstacle avoidance and climbing capability, and mobility in enclosed areas [6]—mostly owing to its designs suitability for omnidirectional motion.

Some of the initial designs that started the research on spherical robots included in Halme et al. [11] and Bicchi et al. [12]. Bhattacharya and Agrawal [13] used two perpendicular rotors, while Joshi and Banavar [14] used four rotors to achieve omnidirectionality by means of conservation of angular momentum and by having internal flywheels that are tilted to induce rolling of the sphere. Gajamohan et al. [15] used three rotors in a cube robot to rotate and balance omnidirectionally. A few spherical robots move by distorting or transforming their outer shell, or by simply using the environment's wind similar to tumbleweed. Sugiyama et al. [16] use shape-memory alloy to deform and roll wheels and spheres, while Wait et al. [17] and Artusi et al. [18] deform panels on a robot's shell via air bladders and dielectric actuators, respectively.

The main difference between the spherical robots that were designed in the past appear to be mainly based on their mechanical driving principles [19]. Despite their desirable features, the challenge with spherical robots stems from trying to solve the complex ball-on-a-plane problem. Therefore, spherical robots tend to require either sophisticated control algorithms and/or limitations imposed on the trajectory planning that they can follow in any indoor or outdoor terrain. For instance, omnidirectionality, one of the most significant advantages of a

spherical robot, may be sacrificed in order to simplify the control problem.

In this paper, we present a spherical robot that has four cable-actuated masses as the propulsion system. The following sections present the overall design of the robot, its equations of motion, and simulation results verifying the derived equations. We conclude with some remarks and discussion for future work.

2. DESIGN

The following sections provide the details on the mechanical design, kinematics, and dynamics of the spherical robot with the cable-actuated driving mechanism.

2.1 Mechanical Design

The design, as depicted in Figure 1, incorporates four tetrahedrally-located motors that move four masses (one per motor) along a straight guide that connects the center of the spherical shell to the inner boundary of the same shell. In order to prevent complications due to any potential slacking of the cables during operation and the rotation of the masses about their sliding axes, slender triangular guide rods are included for each moving mass (Figure 2). The masses are free to move along the guide rail and are moved forward/backward by means of the motors connected to each mass via cables (Figures 1 & 2). The current configuration of the robot has the center of mass at the geometric center of the static mass; therefore, the overall center of mass can be arranged to be at the geometric center any time by locating the masses distributed in a symmetrical manner.

2.2 Kinematics

To describe the dynamics of the four-pendulum mechanism, we define six inertial frames: a static World frame, a Body frame centered on the sphere's center of mass, and four mass frames (numbered 1 to 4) centered on the corresponding point mass. The mechanism and frames are shown in Figure 3.

The Body frame rotates in the World frame using z-x'-z" intrinsic Euler notation with angles ϕ, θ, and ψ, and translates with x and y. For simplicity, the frame is assumed to also be at the sphere's geometric center such that it does not translate in the vertical direction. The homogeneous standard rotation and translation matrices for the Body are $\boldsymbol{R}_\phi$, $\boldsymbol{R}_\theta$, $\boldsymbol{R}_\psi$, and $\boldsymbol{D}_{xy}$, with total transformation from Body to World is:

$$ {}^{W}_{B}\boldsymbol{T} = \boldsymbol{D}_{xy}\boldsymbol{R}_\phi\boldsymbol{R}_\theta\boldsymbol{R}_\psi \tag{1}$$

The sphere's position in the world is:

$$ {}^{W}\boldsymbol{p}_S = {}^{W}_{B}\boldsymbol{T}[0 \quad 0 \quad 0 \quad 1]^{\mathrm{T}} = [x \quad y \quad 0 \quad 1]^{\mathrm{T}} \tag{2}$$

The ith mass frame is defined such that the x_i-axis is aligned with and the z_i-axis is perpendicular to the corresponding guiding rod. The transformation matrix from i to the center of the sphere is:

$$ \boldsymbol{T}_i = \begin{bmatrix} & \boldsymbol{I}_{3x3} & & 0 \\ & & & 0 \\ & & & d_i \\ 0 & 0 & 0 & 1 \end{bmatrix} \tag{3}$$

where d_i is the distance between the center of mass of the sphere and the moving mass on the z_i-axis, and $\boldsymbol{I}_{3x3}$ is the identity matrix. The motors are mounted in a tetrahedral pattern defined by the tetrahedral angle $\varepsilon = \cos^{-1}\left(-1/3\right) \approx 109.5°$ and 120° rotations about the z-axis, represented by rotation matrices (using notation c and s for cosine and sine):

$$ \boldsymbol{R}_\varepsilon = \begin{bmatrix} c\varepsilon & 0 & s\varepsilon & 0 \\ 0 & 1 & 0 & 0 \\ -s\varepsilon & 0 & c\varepsilon & 0 \\ 0 & 0 & 0 & 1 \end{bmatrix} $$

$$ \boldsymbol{R}_{120} = \begin{bmatrix} c120° & -s120° & 0 & 0 \\ s120° & c120° & 0 & 0 \\ 0 & 0 & 1 & 0 \\ 0 & 0 & 0 & 1 \end{bmatrix} \tag{4}$$

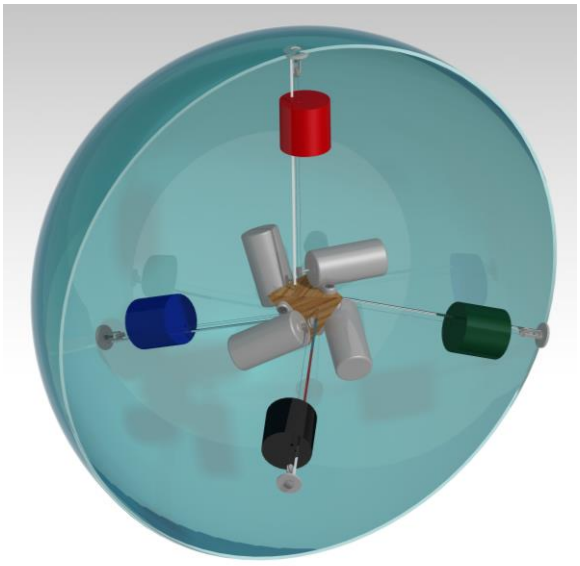

Figure 1. CAD representation of the spherical robot (half of the shell is shown).

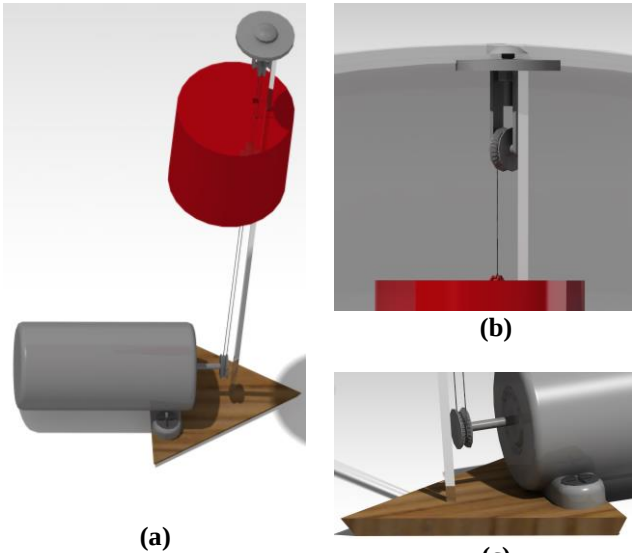

(a) **(b)** **(c)**

Figure 2. (a) Cable-actuation mechanism (shown for a single spoke), (b) Close-up view of the shell connection, and (c) Close-up view of the motor-pulley system.

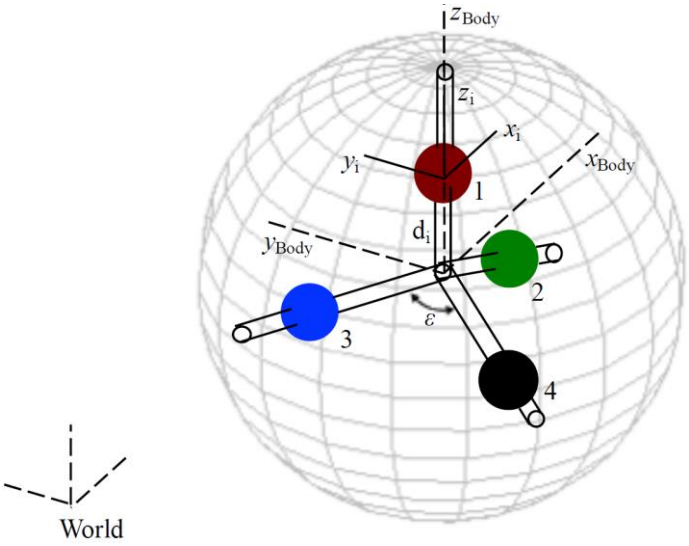

Figure 3. Schematic representation of the driving mechanism (masses are depicted as point masses).

Therefore, the transformations for the four masses are:

$$\begin{aligned} {}^{B}_{1}\boldsymbol{T} &= \boldsymbol{T}_{i=1} \\ {}^{B}_{2}\boldsymbol{T} &= \boldsymbol{R}_{\varepsilon}\boldsymbol{T}_{i=2} \\ {}^{B}_{3}\boldsymbol{T} &= \boldsymbol{R}_{120}\boldsymbol{R}_{\varepsilon}\boldsymbol{T}_{i=3} \\ {}^{B}_{4}\boldsymbol{T} &= \boldsymbol{R}^{\mathrm{T}}_{120}\boldsymbol{R}_{\varepsilon}\boldsymbol{T}_{i=4} \end{aligned} \tag{5}$$

Mass *i* is located at:

$${}^{W}\boldsymbol{p}_i = {}^{W}_{B}\boldsymbol{T}\,{}^{B}_{i}\boldsymbol{T}[0 \quad 0 \quad 0 \quad 1]^T = [x_i \quad y_i \quad z_i \quad 1]^T \tag{6}$$

The system therefore has nine generalized coordinates: the three Euler angles, the two translations, and the four parameters defining the relative distance of the masses with respect to the center of mass of the sphere:

$$\boldsymbol{q} = [\phi, \theta, \psi, x, y, d_1, d_2, d_3, d_4]^T \tag{7}$$

The translational velocities of the sphere and masses are the time derivatives of the $\boldsymbol{p}$ vectors as shown above:

$${}^{W}\dot{\boldsymbol{p}}_s = [\dot{x} \quad \dot{y} \quad 0 \quad 0]^T \tag{8}$$

$$\begin{aligned} {}^{W}\dot{\boldsymbol{p}}_i &= \frac{d}{dt}({}^{W}_{B}\boldsymbol{T}\,{}^{B}_{i}\boldsymbol{T}[0 \quad 0 \quad 0 \quad 1]^T) \\ &= [\dot{x}_i \quad \dot{y}_i \quad \dot{z}_i \quad 0]^T \end{aligned} \tag{9}$$

The mechanism is to be simulated in MATLAB, so it is advantageous to rewrite the ${}^{W}\dot{\boldsymbol{p}}_i$ equation to eliminate time derivatives of functions. This can be done by using the chain rule:

$${}^{W}\dot{\boldsymbol{p}}_i = \left[\frac{\partial {}^{W}\boldsymbol{p}_i}{\partial q_1} \quad \frac{\partial {}^{W}\boldsymbol{p}_i}{\partial q_2} \quad \cdots \quad \frac{\partial {}^{W}\boldsymbol{p}_i}{\partial q_9}\right]\dot{\boldsymbol{q}} \tag{10}$$

The angular velocities of the sphere in World and Body coordinates are:

$$\begin{aligned} {}^{W}\boldsymbol{\omega}_s &= \dot{\boldsymbol{\phi}} + \dot{\boldsymbol{\theta}} + \dot{\boldsymbol{\psi}} = \begin{bmatrix}0\\0\\\dot{\phi}\\0\end{bmatrix} + \boldsymbol{R}_{\phi}\begin{bmatrix}\dot{\theta}\\0\\0\\0\end{bmatrix} + \boldsymbol{R}_{\phi}\boldsymbol{R}_{\theta}\begin{bmatrix}0\\0\\\dot{\psi}\\0\end{bmatrix} \\ &= \begin{bmatrix}\dot{\theta}c\phi + \dot{\psi}s\phi s\theta\\ \dot{\theta}s\phi - \dot{\psi}c\phi s\theta\\ \dot{\phi} + \dot{\psi}c\theta\\ 0\end{bmatrix} = \begin{bmatrix}0 & c\phi & s\phi s\theta & 0\\ 0 & s\phi & -c\phi s\theta & 0\\ 1 & 0 & c\theta & 0\\ 0 & 0 & 0 & 1\end{bmatrix}\begin{bmatrix}\dot{\phi}\\\dot{\theta}\\\dot{\psi}\\0\end{bmatrix}, \end{aligned} \tag{11}$$

and

$$\begin{aligned} {}^{B}\boldsymbol{\omega}_s &= \boldsymbol{R}_{\psi}^{-1}\boldsymbol{R}_{\theta}^{-1}\begin{bmatrix}0\\0\\\dot{\phi}\\0\end{bmatrix} + \boldsymbol{R}_{\psi}^{-1}\begin{bmatrix}\dot{\theta}\\0\\0\\0\end{bmatrix} + \begin{bmatrix}0\\0\\\dot{\psi}\\0\end{bmatrix} \\ &= \begin{bmatrix}s\psi s\theta & c\psi & 0 & 0\\ c\psi s\theta & -s\psi & 0 & 0\\ c\theta & 0 & 1 & 0\\ 0 & 0 & 0 & 1\end{bmatrix}\begin{bmatrix}\dot{\phi}\\\dot{\theta}\\\dot{\psi}\\0\end{bmatrix}. \end{aligned} \tag{12}$$

It is advantageous to define both – as shown later, the World form is needed for the constraint equations, while the Body form is used with the (Body-frame) inertia for the kinetic energy.

2.3 Dynamics

The Lagrange equations of motion and generalized coordinates are

$$\begin{aligned} L &= K_{total} - U_{total} \\ \frac{d}{dt}\left(\frac{\partial L}{\partial \dot{q}_k}\right) - \frac{\partial L}{\partial q_k} &= \sum_{i=1}^{n}\lambda_i a_{ik} + F_k \end{aligned} \tag{13}$$

where L is the Lagrangian, $K_{total}$and U_{total} are the system's kinetic and potential energies, k corresponds to the generalized coordinate (1 to 9), n is the number of constraint equations, the λ's are the Lagrange multipliers for the constraints, the a's are the coefficient in the constraint equations for each generalized coordinate, and the F's are the generalized forces (friction, motor torques, etc.) on the generalized coordinates. Using the chain rule and rewriting following the method described in [20], the equations become:

$$\begin{aligned} \sum_{j=1}^{9}\left(\frac{d\left(\partial K/\partial \dot{q}_k\right)}{dq_j}\dot{q}_j + \frac{d\left(\partial K/\partial \dot{q}_k\right)}{d\dot{q}_j}\ddot{q}_j\right) - \frac{\partial K}{\partial q_k} \\ + \frac{\partial U}{\partial q_k} = \sum_{i=1}^{n}\lambda_i a_{ik} + F_k \end{aligned} \tag{14}$$

where j sums through the generalized coordinates. A third version is useful for control applications:

$$M(\boldsymbol{q})\ddot{\boldsymbol{q}} + \boldsymbol{V}(\boldsymbol{q}, \dot{\boldsymbol{q}}) + \boldsymbol{G}(\boldsymbol{q}) = \sum_{j=1}^{n}\lambda_i a_j + \boldsymbol{F} \tag{15}$$

where $\boldsymbol{M}$ is the inertia matrix, $\boldsymbol{V}$ is the Coriolis and centripetal vector, and $\boldsymbol{G}$ is the gravity vector. The matrix and vectors have the following terms:

$$\boldsymbol{M}_{kj}(\boldsymbol{q}) = \frac{d\left(\partial K/\partial \dot{q}_k\right)}{d\dot{q}_j}$$

$$\boldsymbol{V}_k(\boldsymbol{q},\dot{\boldsymbol{q}}) = \sum_{j=1}^{9}\left(\frac{d\left(\partial K/\partial \dot{q}_k\right)}{dq_j}\dot{q}_j\right) - \frac{\partial K}{\partial q_k} \tag{16}$$

$$\boldsymbol{G}_k(\boldsymbol{q}) = \frac{\partial U}{\partial q_k}$$

The mechanism has static mass *M* (shell, frame, electronics, motors, etc.) and moveable masses of *m* each. The translational ('_*t*') kinetic energies are:

$$K_{s\_t} = \frac{1}{2}{}^{W}\dot{\boldsymbol{p}}_s^T M\,{}^{W}\dot{\boldsymbol{p}}_s = \frac{1}{2}M(\dot{x}^2+\dot{y}^2) \tag{17}$$

$$K_{i\_t} = \frac{1}{2}{}^{W}\dot{\boldsymbol{p}}_i^T m\,{}^{W}\dot{\boldsymbol{p}}_i = \frac{1}{2}M(\dot{x}_i^2+\dot{y}_i^2+\dot{z}_i^2) \tag{18}$$

The sphere has moment of inertia tensor $\boldsymbol{I}_s$ and rotational kinetic energy as:

$$\begin{aligned} K_{s\_r} &= \frac{1}{2}{}^{B}\boldsymbol{\omega}_s^T \boldsymbol{I}_s\,{}^{B}\boldsymbol{\omega}_s \\ &= \frac{1}{2}\left(I_{xx_s}{}^{B}\omega_x^2 + I_{yy_s}{}^{B}\omega_y^2 + I_{zz_s}{}^{B}\omega_z^2\right) \end{aligned} \tag{19}$$

The total kinetic energy is:

$$K_{total} = K_{s\_t} + K_{s\_r} + \sum_{i=1}^{4}\left(K_{i\_t}\right) \tag{20}$$

The total potential energy is the combination of the energy due to the sphere and four masses:

$$U_{total} = U_s + \textstyle\sum_{i=1}^{4} U_i. \tag{21}$$

Where

$$U_s = [0 \quad 0 \quad Mg \quad 0]\cdot {}^{W}\boldsymbol{p}_S = 0 \tag{22}$$

$$U_i = [0 \quad 0 \quad mg \quad 0]\cdot {}^{W}\boldsymbol{p}_i = mgz_i \tag{23}$$

The *R*-radius sphere is assumed to roll without slipping, implementing two nonholonomic constraint equations ($n = 2$):

$$f_1 = \dot{x} - R\cdot {}^{W}\omega_{y_s} = 0 \tag{24}$$

$$f_2 = \dot{y} + R\cdot {}^{W}\omega_{x_s} = 0 \tag{25}$$

The constraint coefficients in the Lagrange Equations can be modeled as:

$$\boldsymbol{a}_1 = \left[\partial f_1/\partial\dot{\phi} \quad \partial f_1/\partial\dot{\theta} \quad \partial f_1/\partial\dot{\psi} \quad 1\ 0\ 0\ 0\ 0\ 0\right]^T \tag{26}$$

$$\boldsymbol{a}_2 = \left[\partial f_2/\partial\dot{\phi} \quad \partial f_2/\partial\dot{\theta} \quad \partial f_2/\partial\dot{\psi} \quad 0\ 1\ 0\ 0\ 0\ 0\right]^T$$

Defining rolling damping as b_r, and motor damping as b_m, the generalized forces can be written as:

$$\boldsymbol{F} = \begin{bmatrix} 0 \\ 0 \\ 0 \\ -b_r \\ -b_r \\ Q_1 - \left(b_m/r_1\right) \\ Q_2 - \left(b_m/r_2\right) \\ Q_3 - \left(b_m/r_3\right) \\ Q_4 - \left(b_m/r_4\right) \end{bmatrix}$$

The generalized force, F_k, for each generalized coordinate can be formulated as:

$$Q_k = \sum_{i=1}^{4} \mathrm{f}_i\,{}^{W}\hat{\mathbf{L}}_i \cdot \frac{\partial {}^{W}\boldsymbol{p}_i}{\partial q_k} \quad k = 1,\ldots,4 \tag{27}$$

Where

$$\begin{aligned} \mathrm{f}_i &= \frac{\tau_i}{r_i} \\ {}^{W}\hat{\mathbf{L}}_i &= {}^{W}_{i}\boldsymbol{T}[0 \quad 0 \quad 1 \quad 0]^T \end{aligned} \tag{28}$$

In the above equation, τ_i is the motor torque that actuates the *i*th mass, r_i is the corresponding radius of the shaft (or pulley attached to the shaft), ${}^{W}\hat{\mathbf{L}}_i$ is the unit vector in the direction of individual d_i expressed in the World coordinate frame.
The equations of motion have been simulated in MATLAB. To simulate the nine coordinate and two constraint equations, the multipliers are solved for using the *x* and *y* equations:

$$\begin{aligned} \lambda_1 &= \boldsymbol{M}_4(\boldsymbol{q})\ddot{\boldsymbol{q}} + \boldsymbol{V}_4(\boldsymbol{q},\dot{\boldsymbol{q}}) + \boldsymbol{G}_4(\boldsymbol{q}) - F_4 \\ \lambda_2 &= \boldsymbol{M}_5(\boldsymbol{q})\ddot{\boldsymbol{q}} + \boldsymbol{V}_5(\boldsymbol{q},\dot{\boldsymbol{q}}) + \boldsymbol{G}_5(\boldsymbol{q}) - F_5 \end{aligned} \tag{29}$$

where the 4 and 5 subscripts signify rows of the matrices and vectors. The multipliers are then substituted back into the remaining seven Lagrange equations (*k* signifies row, from 1 to 3 and 6 to 9):

$$\begin{aligned} &(\boldsymbol{M}_k - \boldsymbol{a}_{1k}\boldsymbol{M}_4 - \boldsymbol{a}_{2k}\boldsymbol{M}_5)\ddot{q} \\ &+(\boldsymbol{V}_k - \boldsymbol{a}_{1k}\boldsymbol{V}_4 - \boldsymbol{a}_{2k}\boldsymbol{V}_5) \\ &\qquad + (\boldsymbol{G}_k - \boldsymbol{a}_{1k}\boldsymbol{G}_4 - \boldsymbol{a}_{2k}\boldsymbol{G}_5) \\ &= (F_k - \boldsymbol{a}_{1k}\boldsymbol{F}_4 - \boldsymbol{a}_{2k}\boldsymbol{F}_5) \end{aligned} \tag{30}$$

The two constraint equations are differentiated (again using the chain rule):

$$\begin{aligned} \frac{df_1}{dt} = \frac{d}{dt}(\boldsymbol{a}_1^T\dot{\boldsymbol{q}}) &= \ddot{\boldsymbol{q}} + \left[\frac{\partial \boldsymbol{a}_1^T}{\partial \boldsymbol{q}}\dot{\boldsymbol{q}}\right]^T\dot{\boldsymbol{q}} \\ &= \boldsymbol{a}_1^T\ddot{\boldsymbol{q}} + \dot{\boldsymbol{q}}^T\frac{\partial \boldsymbol{a}_1}{\partial \boldsymbol{q}}\dot{\boldsymbol{q}} = 0 \end{aligned} \tag{31}$$

$$\frac{df_2}{dt} = \boldsymbol{a}_2^T\ddot{\boldsymbol{q}} + \dot{\boldsymbol{q}}^T\frac{\partial \boldsymbol{a}_2}{\partial \boldsymbol{q}}\dot{\boldsymbol{q}} = 0$$

The differentiation is a standard method (*e.g.*, [21]) and is needed to make the new inertia matrix full rank. These equations are in Eq. (15) form — for example,

$$[\boldsymbol{a}_1^T]\ddot{\boldsymbol{q}} + \left(\dot{\boldsymbol{q}}^T\frac{\partial \boldsymbol{a}_1}{\partial \boldsymbol{q}}\dot{\boldsymbol{q}}\right) + (0) = 0 + 0 \qquad (32)$$

— and can be combined with the seven remaining Lagrange equations. With these modifications, the simulation takes the resulting nine equations, inverts the new inertia matrix, and solves for $\ddot{\boldsymbol{q}}$.

3. SIMULATION RESULTS

The mechanism was symbolically derived in MATLAB and numerically simulated for various initial conditions and motor forces in order to verify the equations of motion. The simulation used normalized values of M = 1.0 (modeled as a homogenous sphere), m = 0.25 (modeled as a point mass), and R=1. The rolling damping and motor damping are assumed zero. Figure 4 shows results from a free-rolling simulation with one mass extended (colored red in the figure). The initial conditions for the simulation are:

$$\boldsymbol{q} = \left[0, \frac{\pi}{2}, \frac{\pi}{2}, 0, 0, R, 0, 0, 0\right]^T$$
$$\dot{\boldsymbol{q}} = [0, -2\pi, 2\pi, 0, 0, 0, 0, 0, 0]^T \qquad (33)$$

Figure 4(a) shows the expected trend of the sphere rolling on its side due to the extended point mass ($d_1 = R$). Figure 4(b) shows the total energy in the system that remains constant as the sphere rolls and curves towards the unbalanced mass. This behavior is expected as there is no work done on the system and all dissipative forces are zero.

An additional method in order to verify the equations of motion during the simulations is checking whether the system constraints are satisfied or not. Figure 4(c) displays the values of the constraint equations that were generated due to the roll without slip condition of the spherical robot. The values shown are obtained by using the equations (24) and (25), which must be equal to zero at all times showing that the roll without slip constraints are satisfied for the considered cases. We observe that numerical solution of these nonlinear and coupled equations of motion introduce very small deviation from zero for these constraint equations (max. -1.6E-4).

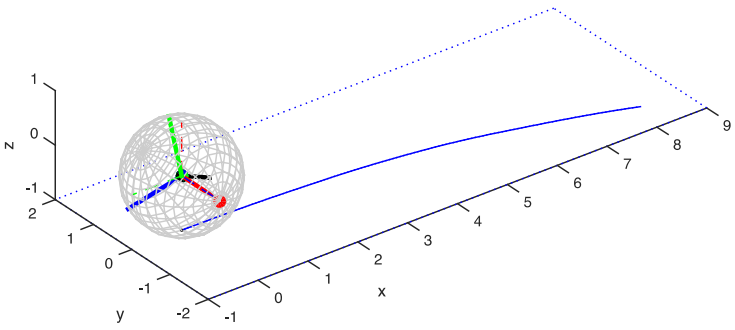

(a)

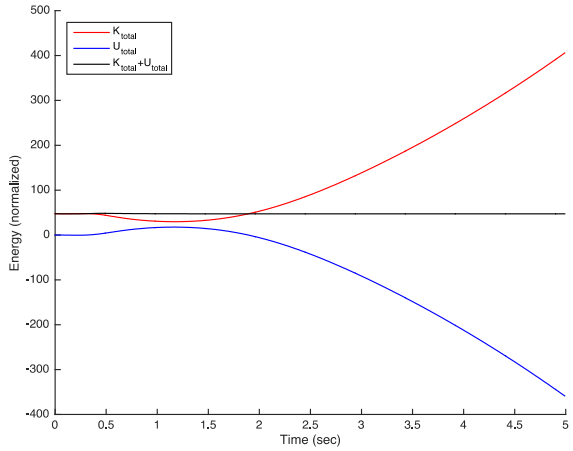

(b)

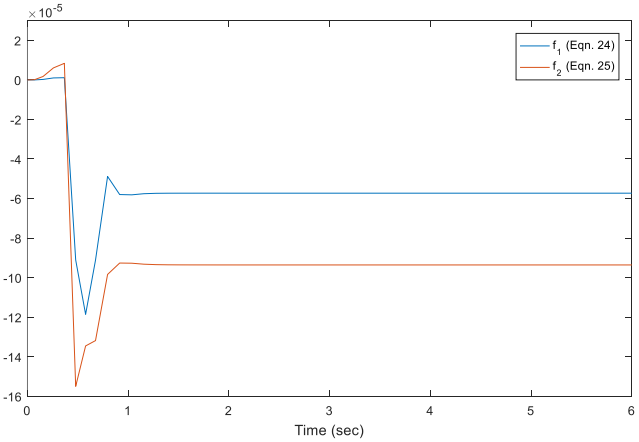

(c)

Figure 4. Simulation results for a free-roll application showing (a) the sphere's trajectory, (b) energy in the system, and (c) the values of the system constraint equations for the no-slip condition.

4. CONCLUSIONS & FUTURE WORK

In this paper, we presented the design of a spherical robot that rolls by shifting its center of mass using four cable-actuated masses. The equations of motions were derived using Lagrange formulation and verified by means of computer simulations.

The specific design presented herein should decrease the overall weight of the robot by using light-weight cables as compared to other mechanisms that use powered-screws to actuate the masses, therefore, providing energy savings that could become imperative at critical tasks such as military and space applications. Along the same lines, the robot's design allows to keep the overall center of mass at the geometric center of the sphere allowing effective tumbleweeding for further energy preservation.

The future work includes creating a control architecture that will permit omnidirectionality without simplifications that potentially may limit the trajectory of the robot, and evaluating this control architecture using a multibody dynamics software such as Simscape™ (Mathworks). Additionally, a prototype is planned to be built and tested for proof of concept.

ACKNOWLEDGMENTS

The authors would like to thank Mr. Thomas Randall, an undergraduate student in the Product Design Engineering Technology (PDET) program at the School of Engineering & Technology at Central Michigan University, for creating the CAD representation of the spherical robot.

REFERENCES

[1] Seeman, M., Broxvall, M., Saffiotti, A., & Wide, P. (2006, October). An autonomous spherical robot for security tasks. In *Computational Intelligence for Homeland Security and Personal Safety, Proceedings of the 2006 IEEE International Conference on* (pp. 51-55). IEEE.

[2] Hogan, F. R., Forbes, J. R., & Barfoot, T. D. (2014). Rolling stability of a power-generating tumbleweed rover. *Journal of Spacecraft and Rockets*,*51*(6), 1895-1906.

[3] Hernández, J. D., Barrientos, J., del Cerro, J., Barrientos, A., & Sanz, D. (2013). Moisture measurement in crops using spherical robots. *Industrial Robot: An International Journal*, *40*(1), 59-66.

[4] Li, M., Guo, S., Hirata, H., & Ishihara, H. (2015). Design and performance evaluation of an amphibious spherical robot. *Robotics and Autonomous Systems*, *64*, 21-34.

[5] Michaud, F., Laplante, J. F., Larouche, H., Duquette, A., Caron, S., Létourneau, D., & Masson, P. (2005). Autonomous spherical mobile robot for child-development studies. *IEEE Transactions on Systems, Man, and Cybernetics-Part A: Systems and Humans*, *35*(4), 471-480.

[6] Armour, R. H., & Vincent, J. F. (2006). Rolling in nature and robotics: a review. *Journal of Bionic Engineering*, *3*(4), 195-208.

[7] Alves, J., & Dias, J. (2003). Design and control of a spherical mobile robot.*Proceedings of the Institution of Mechanical Engineers, Part I: Journal of Systems and Control Engineering*, *217*(6), 457-467.

[8] DeJong, B. P., Karadogan, E., Yelamarthi, K., & Hasbany, (2016). J. Design and Analysis of a Four-Pendulum Omnidirectional Spherical Robot. *Journal of Intelligent & Robotic Systems*, 1-13.

[9] Mojabi, P. (2004). Introducing glory: A novel strategy for an omnidirectional spherical rolling robot. *Journal of Dynamic Systems, Measurement, and Control*, *126*(3), 678-683.

[10] Brown, H. J., & Xu, Y. (1997). A single wheel, gyroscopically stabilized robot. *IEEE Robotics & Automation Magazine*, *4*(3), 39-44.

[11] Halme, A., Schonberg, T., & Wang, Y. (1996, March). Motion control of a spherical mobile robot. In *Advanced Motion Control, 1996. AMC'96-MIE. Proceedings., 1996 4th International Workshop on* (Vol. 1, pp. 259-264). IEEE.

[12] Bicchi, A., Balluchi, A., Prattichizzo, D., & Gorelli, A. (1997, April). Introducing the" sphericle": an experimental testbed for research and teaching in nonholonomy. In *Robotics and Automation, 1997. Proceedings., 1997 IEEE International Conference on* (Vol. 3, pp. 2620-2625). IEEE.

[13] Bhattacharya, S., & Agrawal, S. K. (2000). Spherical rolling robot: A design and motion planning studies. *IEEE Transactions on Robotics and Automation*, *16*(6), 835-839.

[14] Joshi, V. A., Banavar, R. N., & Hippalgaonkar, R. (2010). Design and analysis of a spherical mobile robot. *Mechanism and Machine Theory*, *45*(2), 130-136.

[15] Gajamohan, M., Muehlebach, M., Widmer, T., & D'Andrea, R. (2013). The Cubli: A reaction wheel based 3D inverted pendulum. *IMU*, *2*(2).

[16] Sugiyama, Y., Shiotsu, A., Yamanaka, M., & Hirai, S. (2005, April). Circular/spherical robots for crawling and jumping. In *Robotics and Automation, 2005. ICRA 2005. Proceedings of the 2005 IEEE International Conference on* (pp. 3595-3600). IEEE.

[17] Wait, K. W., Jackson, P. J., & Smoot, L. S. (2010, May). Self locomotion of a spherical rolling robot using a novel deformable pneumatic method. In*Robotics and Automation (ICRA), 2010 IEEE International Conference on*(pp. 3757-3762). IEEE.

[18] Artusi, M., Potz, M., Aristizabal, J., Menon, C., Cocuzza, S., & Debei, S. (2011). Electroactive elastomeric actuators for the implementation of a deformable spherical rover. *IEEE/ASME Transactions on Mechatronics*,*16*(1), 50-57.

[19] Chase, R., & Pandya, A. (2012). A review of active mechanical driving principles of spherical robots. *Robotics*, *1*(1), 3-23.

[20] Karadogan, E., & Williams, R. L. (2013). The Robotic Lumbar Spine: Dynamics and Feedback Linearization Control. *Computational and mathematical methods in medicine*, *2013*.

[21] Murray, R., Li, Z., Sastry, S.S.: A Mathematical Introduction to Robotic Manipulation. CRC Press (1994)

